Discovery, characterization, and pharmaceutical applications of two loratadine- oxalic acid cocrystals

A DISSERTATION

SUBMITTED TO THE FACULTY OF

UNIVERSITY OF MINNESOTA

BY

Zhengxuan Liang

IN PARTIAL FULFILLMENT OF THE REQUIREMENTS

FOR THE DEGREE OF

MASTER OF SCIENCE

Changquan Calvin Sun, Advisor

August/2020

© Zhengxuan Liang 2020

Acknowledgements

It's hard to believe that my two-year journey in the great Pharmaceutics MS program is approaching an end. It is an incredible and fruitful journey full of good memories. Among all the help and kindness I've gotten from the Pharmaceutics faculty, department staff and students, I would like to begin by expressing my appreciation to my adviser, Dr. Changquan Calvin Sun. Back to the time when I joined the Sun group as an undergraduate intern, Dr. Sun showed me around our lab and introduced me to all our lab members, which helped me a lot with integrating into our group and building relationships with those great lab members. Later on, after I joined the Sun lab as a graduate student and started to work with him more closely, I was impressed by his great passion for research and academia. Moreover, he shows me how to be a good researcher. He was a great role model to me on many things, especially his rational and thoughtful research approach and rigorous process in manuscript writing. Again, it's a great honor to have Dr. Sun as my advisor during my graduate study in this great program.

I'm also grateful to have Dr. Timothy Wiedmann and Dr. Chun Wang for their thoughtful opinions and constructive comments as my master's thesis examination committee members.

It's an incredible experience to be a member of the family like group. I thank Dr. Chenguan Wang for those countless days he spent with me, where he provided help and guidance on my projects and experiments. My thanks also go to Dr. Manish Mishra,

who gave me expert advice many times on my research project. Thanks to our lab members Jiangnan, Shenye, Hongbo, Kunlin, Yiwang, Sibo, Zhongyang, Ling, Gerrit and Joan. Thanks for your help, company, informative discussions and interactions. The days working with you will never faded in my memory.

Finally, I appreciate my family and friends for their strong supports especially during this tough time. The memories of my graduate study will last for my whole life. UMN and the Department of Pharmaceutics will always be my second home.

Abstract

Crystallization of multi-component crystals is widely used in pharmaceutical science to enhance the physiochemical properties, such as stability, mechanical properties and solubility. Loratadine (Lor) is a BCS II antihistamine drug commonly used to relieve the symptoms of allergy. It has high permeability but low solubility at physiological pHs. To overcome the problem of low solubility, we synthesized and fully characterized two Loratadine multi-component crystalline phases with oxalic acid (Oxa), i.e., a 1:1 Lor-Oxa conjugate acid-base cocrystal (Lor-Oxa CAB) and a 2:1 Lor-Oxa cocrystal monohydrate (Lor-Oxa hydrate). Both cocrystals exhibited adequate physical stability, enhanced solubility and, higher intrinsic dissolution rate than Lor. The intrinsic dissolution rate of Lor-Oxa CAB is 90 times that of Lor, which makes it a promising candidate for tablet formulation development.

Table of Contents

List of Tables

List of Figures

CHAPTER 1.

INTRODUCTION

1.1 General Introduction

The pharmaceutical sciences is central for converting an active pharmaceutical ingredient (API) into a drug product. [1] The long journey of drug development starts from the discovery of a new chemical entity, which is followed by, among others, sophisticated preformulation and formulation development efforts before it becomes a product. Traditionally, product development is more like an art than a science. Formulations are developed by the trial-and-error approach based on personal experience and redundant data collection, which leads to low efficiency. The quality-by-design (QbD) initiative by FDA stresses the need for more scientific formulation development and scale up.[2] The ultimate goal of developing new drug products for therapeutic performance and benefits requires certain unique properties of the products, which are determined by materials structure. Therefore, understanding structure-property relationship is critical to drug development. Materials Science Tetrahedron (MST) is a conceptual framework that depicts the interdependent relationship among the structure, properties, performance, and processing of a drug.[3]

The successful development of a drug must overcome challenges presented by poor solid-state properties, [4] such as low solubility and poor dissolution performance.[5] Loratadine (Lor) is a drug that faces this problem. Lor is is a second-generation tricyclic H1 antihistamine, used to treat itching, congestion, rhinorrhea, tearing and sneezing by preventing and suppressing the response to histamine or allergen. It is non-sedating, due to the high peripheral selectivity and difficulty to cross the blood-brain

barrier.[6] In 2002, Lor was approved for the over the counter (OTC) status by FDA. [7] Due to its affordable cost and effectiveness, Lor has become the most widely administered antihistamine drug worldwide.

Modifying the solid-state of drug molecules to improve the physical properties of an API is common in drug development because it does not alter pharmacological performances of the molecule upon dissolution.[8] Therefore, the search for new solid forms is valuable part of drug development for developing better medicines.[9] Among all the strategies, the powerful and versatile crystal engineering approach is common adopted to improve API's physical and chemical properties.[10]

The main object of this thesis research is to improve the solubility and dissolution of Lor through identifying suitable solid-state forms enabled by crystal engineering. In this study, we synthesized and characterized two Loratadine multicomponent crystals with oxalic acid, a 1:1 Loratadine-oxalic acid conjugate acid-base cocrystal (Lor-Oxa CAB) and a 2:1 Loratadine-oxalic acid cocrystal monohydrate (Lor-Oxa hydrate). Both crystals exhibited adequate physical stability, enhanced solubility and intrinsic dissolution rate. The more than 90 fold higher intrinsic dissolution rate of Lor-Oxa CAB makes it a promising candidate for further formulation development.

1.2 Solubility and Dissolution Rate

Solubility and dissolution rate are pharmaceutical properties critical for achieving desired bioavailability of poorly soluble drugs. Solubility is the maximum amount of

the substance that is in equilibrium with the solvent phase under a given environment condition. [11] It is a thermodynamic property corresponding to the state of phase equilibration between the solid phase and solution. Solubility of a drug depends on temperature, pressure (of the drug or solvent is a gas), the solute-solvent intermolecular interactions and the polymorphic form of the solid. [12] A supersaturated solution can exist where the solute concentration is above the solubility but will eventually revert to the equilibrium. Poor solubility of drug candidates is a key challenge to pharmaceutical development.[13] Practically, a kinetically controlled meta-stable solubility that is higher than the global thermodynamic solubility may be attained. This is the basis for the common approach of using metastable solid forms to improve the delivery of poorly soluble drugs. The experimentally measured solubility of a poorly soluble drug is sometime underestimated due to the prolonged time period required to establish equilibrium resulting from a slow dissolution rate.[14] Dissolution rate is the rate of individual solute molecules transfer from the solid particles into dissolution media as a free molecule.[15] Many dissolution models have been developed, among all these models, the diffusion layer model is the most pertaining to the dissolution of neat API. In this model, the diffusion generates a concentration gradient between solute surface and the bulk media, which is called diffusion layer. Dissolution rate can be described by the Noyes-Whitney Equation[16]:

$$\frac{dm}{dt} = A\frac{D}{h}(C_s - C_b) \qquad \text{Eq.1-1}$$

Where m is the mass of substance dissolved in the medium at a time t, A is the surface

area of solute particle, D is the diffusion coefficient of the solute in the solvent, h is the thickness of the diffusion layer, C_s is the saturation concentration and C_b is the concentration of the solute in bulk media. From equation 1.1, it can be seen that solubility is a driving force for dissolution rate. When $C_b << C_s$, the dissolution rate is proportional to solubility.[17] For drugs delivered orally, they are normally first dissolved in gastrointestinal fluids before being absorbed. Therefore, the rate of absorption a lipophilic drug is usually limited by the dissolution rate because its dissolved molecules can permeate the membrane quickly.[18] The intrinsic dissolution rate (IDR) is the dissolution rate of a solute normalized by surface area. It can be measured by the rotating disk method.[19] IDR is a kinetic phenomenon rather than an equilibrium phenomenon, so it is affected by several experimental parameters, such as rotation speed. [20]

The Biopharmaceutics Classification System (BCS) II drugs have low solubility and high permeability, composing 60%-70% of drug molecules under development.[21] As low solubility is a limiting factor for the bioavailability of these drugs, several strategies have been developed to improve their solubility, such as cosolvents, surfactants, crystal engineering, amorphous solid dispersions, cyclodextrins, solid lipid nanoparticles, and other colloidal drug delivery systems[22]

1.3 Tablets and Tablet Strength

The tablet dosage form usually contains API and suitable pharmaceutical excipients prepared either by compression or moulding.[23] It is the most commonly used

pharmaceutical dosage form that account for more than 80% of all dosage forms administered to humans.[24] [25] The popularity of tablets can be attributed to their advantages in both manufacturing and administration, including accurate dose, stability, easy to handle and storage, lower manufacturing cost than other dosage forms, and possibility for high volume production.[26] For the patients, the tablets are easy to administer and may be divided into halves or quarters when a fractional dose is required. [24] Specially designed tablets with modified-release or specific route of administration are also possible.[27] For Lor, swallowable, chewable, and orally disintegrating tablets have been marketed.

A good tablet product should meet the criteria of stability, content uniformity, manufacturability, bioavailability, bioequivalency (for a generic product), pharmaceutical elegance, and low cost if possible. [28] Adequate mechanical strength is required for a tablet to survive downstream processing, handling and shipping, averting unacceptable loss of drug content, [29-30] but excessive strength could lead to longer distinguish time and slower drug release or make the tablets too hard to break. [5] Solid state properties (e.g., hygroscopicity, solid form, crystal structure), mechanical properties (e.g., plasticity, elasticity, brittleness) and powder properties (e.g., particle size and shape, surface energy) can all influence the tableting behavior of APIs.[31] Therefore, the first step of tablet design or formulation development is to have a full understanding of the physicochemical properties of the API.

Tabletability, compressibility, and compactibility reveal the relationships among

compaction pressure, tensile strength (TS), and solid fraction (porosity) (Figure 1.1), which are critical to understand the compaction behavior.[32] Tensile strength can be understood based on the qualitative bonding area (BA)-bonding strength (BS) model, where contributions of BA and BS are simultaneously considered.[5] BS accounts for intermolecular interactions, mainly including van der Waals and hydrogen bonds for molecular solids. During the consolidation of a powder, particles undergo permanent deformation to result in BA. Hence, BA depends on compaction conditions, mechanical properties (plastic, elastic), and particle properties (e.g., size, shape). BA and BS can be assessed by compressibility and compactibility, respectively. Both larger BA and BS favor higher TS.

1.4 Crystal Engineering

The concept "crystal engineering" was first mentioned in 1955, [33] and officially appeared in the literature in 1971 when Gerhard Schmidt listed "crystal engineering" as one of the four concurrent and connected phases of solid-state photochemical research.[34] Crystal engineering may be defined as "*The understanding of intermolecular interactions in the context of crystal packing and the utilization of such understanding in the design of new solids with desired physical and chemical properties*"[10]. The intermolecular interactions formed the smallest structural units, supramolecular synthons, through which molecules assemble into supramolecules. [35] There are four steps in crystal engineering: observation of structural groups, rationalization of crystal packings, prediction of new structures, and testing of the

predictions[35] With the unremitting invention of the crystallographic techniques, crystal engineering went over a rapid development. Today, it is widely used in multi fields including chemistry, material science and pharmaceutical science.

In pharmaceutical sciences, crystal engineering is utilized to obtain desirable mechanical and physicochemical properties of drug compounds without altering their pharmacological performances [36] through the methods of habit modification, surface modification, polymorphism, solvation formation, and cocrystalization.[37] Among all the techniques, cocrystallization has been widely used to improve the physicochemical properties of pharmaceutical compounds, including physical stability (sublimation tendency, and hydration tendency)[38-39], chemical stability, solubility[40] and dissolution[41], mechanical properties[29], permeability[42], and punch sticking propensity.[43] Such multi-component crystals exploit noncovalent interactions between neutral molecular or ionic components with a well-defined stoichiometry in a solid-state structure[44]. Hydrogen bonding is one of the most important interactions for designing a cocrystal. Etter proposed the following Hydrogen-Bond Rules based on the examination of functional groups and hydrogen-bond patterns in a vast number of crystals [45]: "*1. All good proton donors and acceptors are used in hydrogen bonding. 2. Six-membered ring intramolecular hydrogen bonds form in preference to intermolecular hydrogen bonds. 3. The best proton donor and acceptor remaining after intramolecular hydrogen-bond formation will form intermolecular hydrogen bonds to one another."*

CHAPTER 2.

DISCOVERY, CHARACTERIZATION, AND PHARMACEUTICAL APPLICATIONS OF TWO LORATADINE- OXALIC ACID COCRYSTALS

Overview

Loratadine (Lor) is a BCS II antihistamine drug commonly used to relieve the symptoms of allergy. It has high permeability but low solubility at physiological pHs. In this study, we synthesized two Lor multicomponent crystals with oxalic acid (Oxa), i.e., 1:1 Lor-Oxa conjugate acid-base cocrystal (Lor-Oxa CAB) and 2:1 Lor-Oxa cocrystal monohydrate (Lor-Oxa hydrate). Both Lor-Oxa crystals exhibited adequate physical stability, enhanced solubility and intrinsic dissolution rate (IDR). Overall results suggest that Lor-Oxa CAB is a promising candidate for further tablet formulation development because of its much higher (95 fold) dissolution rate than Lor.

2.1 Introduction

Low aqueous solubility is a major challenge to the design of oral solid forms.[46] It may lead to poor drug bioavailability because of the slow dissolution process before drug molecules can be absorbed into the systemic circulation. Many approaches have been developed to enhance solubility or dissolution, including particle size reduction, cosolvents, surfactants, more soluble crystal forms, amorphous solid dispersions, cyclodextrins, solid lipid nanoparticles, and other colloidal drug delivery systems.[22] Cocrystallization is a crystal engineering technique widely used in pharmaceutical research and development of drugs.[44, 47] It exploits noncovalent interactions between neutral or ionic components with a well-defined stoichiometry in a solid-state structure,[9] which could improve the physicochemical properties of active pharmaceutical ingredients (API), including physical stability (sublimation tendency, and hydration tendency)[38-39], solubility[40] and dissolution[41], mechanical properties[29], permeability[42] , and punch sticking propensity.[43, 48]

Loratadine (Lor) (Figure 2.1.a) is a second-generation tricyclic H1 antihistamine, used to treat itching, congestion, rhinorrhea, tearing and sneezing by preventing and suppressing the response to histamine or allergen. Its non-sedating nature, due to the high peripheral selectivity and low ability to cross the blood-brain barrier, makes it a medicine of choice for treating allergies.[6] Lor is a weakly basic drug (pKa = 5.25),[49] belonging to the Biopharmaceutical Classification System (BCS) Class II.[50] The solubility of Lor decreases exponentially with increasing pH, which partially results in

high variability in pharmacokinetic parameters. [50-51] The solubilty of Lor in pH 6/8 phosphate buffer is 0.7 mg/L.[52] Given the wide use of Lor, a new crystal form of Lor with improved solubility and dissolution rate, which reduceds variability in bioavailability, as well as enhanced powder properties for more efficient pharmaceutical processing is desired for developing new Lor tablets with better in vivo performance.[53] Past efforts to improve the solubility of Lor include the use of complexes [54-55], solid dispersion[56-57], solid lipid microparticles[58], solid lipid nanoparticles[59], self microemulsifying particles,[60] and coamorphous systems.[61] However, the cocrystal/salt approach has been so far unsuccessful.[62]

In this study, a series of organic acids, as potential coformers or salt former, were screened. Two new multicomponent crystalline forms of Lor (Figure 2.1.b) were discovered, i.e., a Lor - Oxalic acid (Oxa) conjugate acid-base salt (Lor-Oxa CAB) with the Lor to Oxa ratio of 1: 1 and Lor-Oxa cocrystal monohydrate (Lor-Oxa hydrate, Lor:Oxa = 2:1). The pharmaceutical properties, including crystal structure, dissolution, thermal property, physical stability and mechanical property, of both new crystal forms were characterized for suitability to develop a tablet product with a faster and more robust drug release performance and manufacturability. Both new cocrystals exhibited enhanced solubility and intrinsic dissolution rate (IDR). However, ~95 fold IDR of Lor-Oxa CAB than Lor makes it a more attractive crystal form for further tablet formulation development.

2.2 Materials and Methods

2.2.1 Materials

Loratadine was purchased from; Wuhan Biocar Bio-pharm Co. Ltd. (Wuhan, Hubei, China). Oxalic acid, resorcinol, malonic acid, benzoic acid, DL-malic acid, nicotinic acid, and succinic acid were all purchased from Sigma−Aldrich (St. Louis, MO) and were used as received. Microcrystalline cellulose (MCC; Pharmacel 102) was provided by DFE Pharma (Goch, Germany).

2.2.2 Screen for Loratadine Salt/Cocrystals

Each candidate carboxylic acid was suspended with Lor, in 1:1 molar ratio, in various solvents, including ethanol, ethyl acetate, isopropanol, methanol, and acetone. 1 mmol of each of Lor and a carboxylic acid powders were fully dissolved in 5 mL of a solvent in a vial with heating. The vial was then left open in a fume hood to allow solvent to evaporate. The resulting solid was characterized by powder X-ray diffraction (PXRD) to identify possible new crystal form.

2.2.3 Single Crystal Preparation

Equimolar Lor (765.76 mg, 2 mmol) and Oxa (180.08 mg, 2 mmol) or 2:1 molar ratio Lor (765.76 mg, 2 mmol) and Oxa (90.04 mg, 1 mmol) were dissolved in 6 mL of acetone. The vials were left in a cold room (4^{o}C), covered by parafilm with holes introduced to allow slow evaporation of the solvent and crystal growth. Crystals suitable for single crystal X-ray diffraction study were harvested within one week. Lor-

Oxa CAB and Lor-Oxa hydrate were obtained form 1:1 and 2:1 samples, respectively.

2.2.4 Single Crystal X-Ray Diffractometry (SCXD)

A Bruker-AXS Venture Photon-II diffractometer (Bruker AXS Inc., Madison, Wisconsin), with a Photon-II (CMOS) detector, was used to collect the SCXRD data at 100 K using Mo Kα radiation (graphite monochromator). A suit of software, including APEX3, SADABS and SAINT, was used for data analysis. The structures were solved using SHELXT 2014 program and refined using SHELXL 2018 program. Based on systematic absences and intensity statistics, the space group $P2_1/c$ was determined. A direct-methods solution was calculated, which provided most non-hydrogen atoms from the E-map. Full-matrix least-squares/difference Fourier cycles were performed to locate the remaining non-hydrogen atoms. All non-hydrogen atoms were refined with anisotropic displacement parameters. All hydrogen atoms were placed in ideal positions and refined as riding atoms with isotropic displacement parameters.

2.2.5 Bulk Powder Preparation

Bulk powder of Lor-Oxa CAB was prepared by completely dissolving 4.59 g of Lor (12 mmol) and 1.08 g of Oxa (12 mmol) in 15 mL of acetone at room tempeature. The slution was placed in a cold room (4 ºC) with continuous stirring for 24 h. The precipitant was then washed with acetone, filtered, and dried in a 35 ºC oven for overnight. A bulk powder of Lor-Oxa hydrate was prepared in a similar way, except 4.59 g of Lor (12 mmol) and 0.54 g of Oxa (6 mmol) was dispersed in 15 mL of acetone

and slightly heated to obtain a clear solution before the sample was placed in the cold room.

2.2.6 Powder X-ray Diffractometry (PXRD)

Powder X-ray diffractograms were collected using a powder X-ray diffractometer (X'pert Pro; PANalytical, Westborough, MA) equipped with Cu Kα radiation (1.54059 Å). Samples were scanned between 5 to 30° 2θ with a 0.02° step size and a 1 s/step dwell time at ambient temperature. The tube voltage and amperage were set at 45 kV and 40 mA, respectively.

2.2.7 Thermal Analysis

The thermal properties of powders were characterized by thermogravimetric analysis (TGA) and differential scanning calorimetry (DSC).

DSC data was collected using a thermogravimetry analyzer (Model Q500, TA Instruments, New Castle, DE, USA). Powder samples (approximately 3 mg) were heated in open aluminum pans from room temperature to 300 °C at 10 °C/min under 60 mL/min dry nitrogen purge.

DSC data was collected on a differential scanning calorimeter (Q1000, TA Instruments, New Castle, DE, USA). Powder samples (~3 mg) were loaded into hermetically sealed aluminum Tzero pans and heated with a heating rate of 10 °C/min from room temperature to 150 ºC under dry nitrogen purge at a flow rate of 50 mL/min.

To assess the stability of Lor-Oxa hydrate, a powder sample was placed in a 100 ºC oven. An aliquot of powder was taken out for PXRD analysis after 1, 2, 3, 4, 5, 6, 12, and 18 days.

2.2.8 Hot Stage Microscopy (HSM)

HSM was performed with a polarized light microscopy (Eclipse e200; Nikon, Tokyo, Japan). Images of crystals were captured by a DS Fi1 microscope digital camera. Crystals were heated to 150 ºC at the rate of 5 °C/min with a temperature controller (Linksys 32; V.2.2.0, Linkam Scientific Instruments, Ltd., Waterfield, UK).

2.2.9 Fourier Transformation Infrared Spectroscopy (FT IR)

FT-IR spectra (in the range of 4000−400 cm^{-1}) of dry powders were obtained using a FT-IR spectrometer (NicoletiS50; Thermo Scientific, Waltham, MA) equipped with a diamond attenuated total reflection (ATR) and DLaTGS detector. The spectrum of each sample was an average of 32 scans with a spectral resolution of 2 cm^{-1}. Data processing was performed with the OMNIC 9.2 software.

2.2.10 Moisture Sorption and Desorption

Isothermal water sorption and desorption isotherms were collected using an automated vapor sorption analyzer (Intrinsic DVS, Surface Measurement Systems Ltd., Allentown, PA, USA) at 25°C with nitrogen flow rate of 50 mL/min. Sample weight was monitored by a micro balance. The Lor-Oxa CAB sample was first purged with

dry nitrogen until a constant weight was obtained. The RH was varied from 0% to 95% during sorption followed by 95% to 0% during desorption with a step size of 5% RH. For Lor-oxa hydrate, the powder sample was exposed to a series of relative humidities (RH) from 95 % to 0% then back to 95% with a step size of 5% RH. Samples were equilibrated at each step with the equilibration criteria of either dm/dt = 0.003% or maximum equilibration time of 6 h was reached before changing to the next target RH.

2.2.11 Solubility and Intrinsic Dissolution Rate (IDR)

Solubility was determined by suspending an excess amount of a solid (100 mg) in 5 mL of pH 6.8 phosphate buffer under stirring at 25 °C for 72 h. Each suspension was passed through a 0.45 μm PTEE membrane filter. The filtrate was appropriately diluted with the medium for measurement by a UV−vis fiber optic probe (Ocean Optics, Dunedin, FL) at 250 nm. Solution concentration was calculated based on a previously constructed calibration curve (Figure 2.2). The residual solids were collected and tested by PXRD to verify the solid phase.

The IDR was determined by the rotating disc method[63 64] in a phosphate buffer at pH 6.8 to mimic duodenum pH. For each sample, approximately 20 mg of powder was compressed at a force of 2000 lb, using a custom-made stainless-steel die, against a flat stainless-steel disc for 2 min to prepare a pellet (6.39 mm in diameter). The surface of the pellet was visually smooth and coplanar with the die surface. While rotating at 200 rpm, the die was immersed in a 200 mL dissolution medium at 37°C in a water-jacketed beaker. An UV−vis fiber optic probe (Ocean Optics, Dunedin, FL) was used

to continuously monitor the UV absorbance of the solution at λ = 250 nm. IDR was calculated from the slope of the linear portion of the concentration time profile and the pellet surface area exposed to the dissolution medium. PXRD of the pellet after IDR was collected to either confirm or eliminate the possibility of phase transition during dissolution.

2.2.12 Tabletability

Powder compaction was carried out using a universal material testing machine (model 1485; Zwick/ Roell, Ulm, Germany). To minimize the effect of particle size, powder samples were ground in a mortar with a pestle and passed through a # 60 mesh (≤ 250 μm) sieve before compaction. Particle sizes were assessed by polarized light microscopy. Three mixtures conatining 25% (w/w) of one of the three Lor crystal forms and 75% (w/w) of MCC PH102, were blended using a Turbula mixer (Glen Mills Inc., Clifton, NJ) for 5 min at 49 rpm. Tablets were compacted under pressures ranging from 25 to 350 MPa at a speed of 4 mm/min, using flat faced round punches (8 mm diameter). For pure crystal forms, the punch tip and die wall were lubricated with a suspension of magnesium stearate in ethanol (5% w/v) and air dried prior to each compaction. For mixtures with MCC, no lubricant was used because the low tendency of punch sticking and low ejection force. Tablets were relaxed for at least 24 h in a tightly closed glass vial before their dimensions were measured and broken diametrically with a texture analyzer (TA-XT2i; Texture Technologies Corporation, Scarsdale, NY). Tablet tensile strength (σ) was calculated using Eq. 2-1.[65]

$$\sigma = \frac{2F}{\pi Dh} \quad (2\text{-}1)$$

Where F is the breaking force, D is tablet diameter, and h is tablet thickness.

Powder true density was measured using a helium pycnometer (Quantachrome Instruments, Ultrapycnometer 1000e, Byonton Beach, Florida). Approximately 1 g of each powder was accurately weighed and placed into a sample cell (10 mL cell volume). The measurement was stopped when the coefficient of variation of the last five consecutive volume measurements was less than 0.005% or after 100 measurements, in which case the last five measurements were used to calculate an average and standard deviation. Tablet porosity (ε) was calculated using Eq. (2-2):

$$\varepsilon = 1 - \frac{\rho}{\rho_t} \quad (2\text{-}2)$$

where ρ and ρ_t are tablet density and powder true density, respectively.

2.3 Results and Discussion

2.3.1 Crystal Screening and Structure Analysis

Slurrying Lor and Oxa at 2:1 and 1:1 molar ratios led to two PXRD patterns different from those of the starting Lor and Oxa, suggesting that new solid forms were obtained (Figure 2.3).

Single crystal structures solved by SCXRD confirmed they are new crystalline complexes between Lor and Oxa. When crystallized from the 1:1 Lor:Oxa solution,

the crystal belongs to the $P2_1/c$ space group of the monoclinic system. Its unit cell consisted of six asymmetric units (Z=6). The asymmetric unit is consisted of cationic Lor^+, anionic Oxa^-, and neutral Oxa at the molar ratio of 2:1:1 (Figure 2.4 a). Key crystallographic information is summarized in Table 2.1. In this structure, 1D Oxa chains running along the *b* axis were formed via hydrogen bonds of O-H···O^- (2.510, 2.512, 2.515 Å)（Figure 2.4b). The Oxa chains are connected with Lor^+ through N^+-H···O=C (2.624, 2.726 Å) and N^+-H···O^- (2.897, 2.988 Å) (Figure 2.4c). The adjacent chains formed a 2D layer structure through π···π (3.439 Å), Cl···π (3.320 Å) stacking, and C=O···H-C (3.402 Å) hydrogen bond along the (-1 0 -2) plane. The adjacent layers stack to form a 3D packing structure, stabilized by weak C-H···O (3.520 Å) hydrogen bonds (Figure 2.4d).

When crystallized from the 2:1 Lor:Oxa solution, the crystalline phase also belongs to the monoclinic P21/c space group. Its unit cell contains 4 asymmetric units (Z=4), each comprised of 1 Lor, 0.5 Oxa (Oxa has an axis of symmetry), and one water molecue (Figure 2.5 a). Key crystallographic information is summarized in Table 2.1. Lor and water interact via C=O··· H-O (2.977 Å) and O-H···Cl (3.232 Å) hydrogen bonds to form 1D chains(Figure 2.5 b). One Oxa molecule further connects to two Lor molecules in adjcent chains via O-H···N (2.609 Å), C-H···O=C (3.322 Å), C··H-O (3.448 Å, 3.528 Å) hydrogen bonds (Figure 2.5 c) to form 2D zig-zaged layers. Finally, the layers stack to form a 3D packing structure. (Figure 2.5 d)

The calculated PXRD patterns of the two new solid forms matched well with the

PXRD patterns of the solids obtained from the slurry method (Figure 2.3).

2.3.2 Formation Conditions of the Two Crystals

Given that Lor-Oxa CAB could be obtained at 1:1 Lor to Oxa ratio, and Lor-Oxa hydrate was prepared at 2:1 ratio. The amount of Oxa is expected to play a key role in phase stability of both crystals. Slurry experiments at different Lor to Oxa ratios suggested that Lor to Oxa ratio did affect solid form, as shown by the PXRD patterns (Figure 2.6). Phase change was monitored using unique peaks of Lor at 7.52 degree two-theta (marked with a yellow dashed line), Lor-Oxa CAB at 10.04 degree two-theta (marked with a blue dashed line) and 19.93 degree two-theta (marked with green dashed line), Lor-Oxa hydrate at 8.87 degree two-theta (marked with a black dashed line). At ratio 1:0.2, the product is a mixture of Lor and Lor-Oxa hydrate. For 1:0.3 to 1:0.5 ratios, pure Lor-Oxa hydrate was obatined. At 1:0.6 to 1:0.9 ratios, the powders are mixtures of Lor-Oxa hydrate and Lor-Oxa CAB, where the amount of Lor-Oxa CAB increases with increasing Oxa amount. When the Lor to Oxa ratio reaches 1:1, the product is pure Lor-Oxa CAB form.

2.3.3 Solid State Characterization

Differential scanning calorimetric (DSC) thermograms of Lor-Oxa CAB exhibited a single endotherm with an onset temperature of 124.29 °C (ΔH_f = 69.78 J/g) and peak temperature of 129.72° (Figure 2.7 a). The TGA profile (Figure 2.7 b) showed negligible weight loss below 150 °C, suggesting acceptable thermal stability. This is important for further tablet development, which may involve drying.[66] Signifiant

weight loss was observed at ≥ 150 ºC, likely due to the evaporation of Oxa from the melt. A Lor-Oxa CAB single crystal melted at 135 ºC in a HSM study (Figure 2.7 c), the higher melting point by HSM than that by DSC is attributed to the thermal lag during the HSM experiment.

The weight loss of Lor-Oxa hydrate corresponds to dehydration, which initiated at around 92 ºC and proceeds slowly until the accelerated weight loss at ≥112 ºC (Figure 2.7 b). The DSC thermogram of Lor-Oxa hydrate exhibited two overlapping endotherms with onset temperature of 119.84 °C (ΔH f = 93.88 J/g) (Figure 2.7a). The onset temperature of the DSC endotherm is ~28 ºC higher than the temperature corresponding to the initial weight loss observed on TGA. This temperature difference is larger than expected, which may partially result from the depression of the dehydration reaction by the build up of water vapor from the initial dehydration in DSC pan. A Lor-Oxa single crystal released water bubbles when heated to 101 ºC and continued through the melting of the crystal in the temperature range of 130 - 136 ºC (Figure 2.7 d). This is consistent with the significant overlap of the two endotherms observed in the DSC thermogram of Lor-Oxa (Figure 2.7a).

The FT-IR spectra of Lor, Oxa, and two Lor cocrystals show distinct peaks (Figure 2.8). The strongest sharp absorption band at 1698 cm^{-1} of the Lor is attributed to the C=O of the ester group, which is distinct from the broad C=O absorption bands of the two carboxylic acid groups with a peak position at 1668 cm^{-1}. The larger red-shift of Lor-Oxa hydrate (26 cm^{-1}) than Lor-Oxa CAB (9 cm^{-1}) of the C=O peak can be

explained by the O-H···O (2.977 Å) hydrogen bond formation between ester C=O and water. The $\geqslant$100 cm^{-1} red-shift of the C=O absorption band of a fully deprotonated carboxylate group [67] was not obvious in the FTIR spectra of both Lor-Oxa hydrate and Lor-Oxa CAB because of the overlapping of the much stronger C=O absorption bands of Lor. The low intensity of O-H absorption bands of Oxa in Lor-Oxa CAB is attributed to its participation in strong charge assisted hydrogen bonds of O-H···O^- (2.510, 2.512, 2.515 Å) and absence of water. In contrast, the hydroxyl groups of water and Oxa in Lor-Oxa hydrate only participate in weak hydrogen bonds (O-H···O, 2.977 Å; O-H···Cl, 3.232 Å).

2.3.4 Moisture Sorption and Desorption Behavior.

Both Lor-Oxa CAB and Lor-Oxa hydrate gained less than 1% weight up to 95% RH and only slight hysterisis between sorption and desorption curves was observed (Figure 2.9). Therefore, the weight change of both samples is due to the surface adsorption not hydration/dehydration. The physical stability of Lor-Oxa hydrate against changes in RH is consistent with the thermal data (Figure 2.7), which suggests that dehydration did not occur under dry nitrogen purge until temperature was at least 92 ºC. When stored at a 100 ºC oven, Lor-Oxa hydrate did not undergo detectable dehydration after 1 day base on PXRD (Figure 2.10). Characteristic peaks of Lor, e.g., 12.7 º two theta, appeared after two days. However, an appreciable amount of Lor-Oxa hydrate remained even after 6 days. Complete conversion to Lor was observed after 12 days. The stability of Lor-Oxa hydrate is attributed to the

stabilization of water in the crystal structure by forming C=O···H-O (2.977 Å) and O-H···Cl (3.232 Å) hydrogen bonds. Therefore, Lor-Oxa hydrate could be used in typical pharmaceutical manufacturing and storage conditions without a high risk of phase change.

2.3.5 Solubility and Intrinsic Dissolution Rate

Both solubilities and dissolution rates of the two new crystal forms of Lor are determined in pH 6.8 phosphate buffer to mimic the human physiology environment. During solubility measurement at 25 ºC, Lor-Oxa CAB converted to Lor-Oxa hydrate within three days while Lor-Oxa hydrate remained stable. The phase change suggests that Lor-Oxa CAB is more soluble than Lor-Oxa hydrate in the pH 6.8 buffer.[68]

Compared to Lor, Lor-Oxa hydrate displays both improved solubility (1.46×) and intrinsic dissolution rate (1.85×) (Figure 2.12 a.b, Table 2.2). Lor-Oxa CAB exhibits a much higher IDR, about 95 times of Lor. In the IDR curve of Lor-Oxa CAB, the concentration of Lor in the medium initially increased linearly up to a concentration of 11.36 ±0.37 μg/mL and then decreased (Figure 2.14). The PXRD pattern of the Lor-Oxa CAB pellet after IDR experiment matched that of Lor-Oxa hydrate, indicating conversion to Lor-Oxa hydrate (Figure 2.12 c). The decline in the concentration of Lor beyond 10 min suggests bulk precipitation, which explains the observed turbidity of the dissolution medium (Figure 2.12 d). Since the degree of supersaturation is the highest at the surface of pellet, free drug tends to precipitate out more easily at the pellet surface than in the bulk. Thus, Lor-Oxa CAB is a good model compound to

study the bulk precipitation phenomenon. Potential reasons for bulk precipitation include: (a) The high dissolution rate leads to faster receding of the pellet surface than the time required to form nuclei in absence of a solid surface; and (b) the pH in the diffusion layer is lower than that in the bulk medium, which leads to a lower degree of supersaturation of Lor since the solubility of Lor is higher at a lower pH.

2.3.6 Tabletability

Tabletability is an important property of drugs for successful tablet formulation, especially when the drug loading is high.[69] Both new Lor crystal forms exhibited reduced tabletbility than Lor over the entire compaction pressure range of 25 – 350 MPa (Figure 2.15 a). The tablet tensile strength of Lor-Oxa CAB increased with increasing pressure up to 200 MPa, beyond which higher pressure led to slightly lower tensile strength. Similar observation occurs for the Lor-Oxa hydrate, although the decline in tensile strength occurred at pressures higher than 100 MPa. At 350 MPa, intact tablets of Lor-Oxa hydrate could not be made due to extensive lamination of tablets (Figure 2.15 a). Such lamination suggests extensive elastic recovery during decompression stage of the tableting cycle, which breaks bonding sites formed between particles during compression.[70] To understand their difference on tableting performance, compressibility and compactibility profiles are also compared (Figure 2.15b,c). At any given compaction pressure, the porosity of Lor tablets was always lower than those of the two new crystal forms, which were similar (Figure 2.15b). This suggests that the bonding area between Lor particles was larger than the two new

crystals, since the particle size and shape among them were similar (Figure 2.16). Interestingly, the apparent bonding strength, σ_0 (tablet tensile strength at 0 porosity), of Lor-Oxa hydrate is the highest, followed by Lor and Lor-Oxa CAB (Figure 10c). Therefore, the higher tabletabillity of Lor is attributed by the larger bonding area not higher bonding strength according to the bonding area – bonding strength interplay model of tablet tensile strength.[71]

When mixed with MCC, all three solid forms of Lor exhibited good tabletability, following the descending order of Lor > Lor-Oxa CAB > Lor-Oxa hydrate (Figure 2.17). All mixtures could form tablets with tensile strength of 2 MPa at pressures below 100 MPa. Given the drug loading in the commercial Lor tablet products is around 2% because of the low dose of Lor (10 mg), no issue with tablet mechanical strength is expected for any of the three crystal forms with a suitable formulation. [2]

2.4 Conclusions

We have discovered and characterized two new multi-component crystalline forms of Lor with Oxa. Both crystal forms exhibit acceptable stability for drug development. Although both exhibit improved solubility and dissolution rate, Lor-Oxa CAB is much more soluble than Lor-Oxa hydrate. Therefore, Lor-Oxa CAB is the preferred crystal form for tablet formulation development although the Lor-Oxa hydrate is also suitable if desired. However, the potential phase transition of Lor-Oxa CAB to Lor-Oxa hydrate during dissolution needs to be examined carefully to avoid unexpected dissolution failure.

Table 2.1. Crystallographic data for Lor-Oxa CAB and Lor-Oxa hydrate

	Lor-Oxa CAB	**Lor-Oxa hydrate**
Formula	C48H50Cl2N4O12	C23H26ClN2O5
Formula weight	945.82	445.91
Temperature/K	100	100
Crystal system	Monoclinic	Monoclinic
Space group	p21/c	p21/c
a, Å	16.5860(8)	9.1806(3)
b, Å	10.61335(5)	11.4581(3)
c, Å	38.1283(17)	20.1427(6)
a, deg	90	90
b, deg	94.606(2)	94.084(1)
g, deg	90	90
Volume, $Å^3$	6690.1(5)	2113.48(11)
Z	6	4
Dc/$g.cm^3$	1.409	1.401
F(000)	2976.0	940
R1 [I > 2σ(I)]	0.0550	0.0552
*wR*2 [*I*>2sigma(*I*)]	0.1291	0.1647

Table 2.2 Solubility at 25 °C (n = 3) and Intrinsic Dissolution Rate of Lor, Lor-Oxa CAB, Lor-Oxa hydrate at 37 °C (n = 3) in pH 6.8 phosphate buffer

Material	**Lor**	**Lor-Oxa CAB**	**Lor-Oxa hydrate**
Solubility(mg·L^{-1})	0.7±0.0	--	1.149±0.038
IDR (μg·cm^{-2}·s^{-1})	$2.316*10^{-4}$ $\pm1.6*4710^{-5}$	$2.201*10^{-2}$ $\pm4.839*10^{-4}$	$4.282*10^{-4}$ $\pm2.164*10^{-5}$

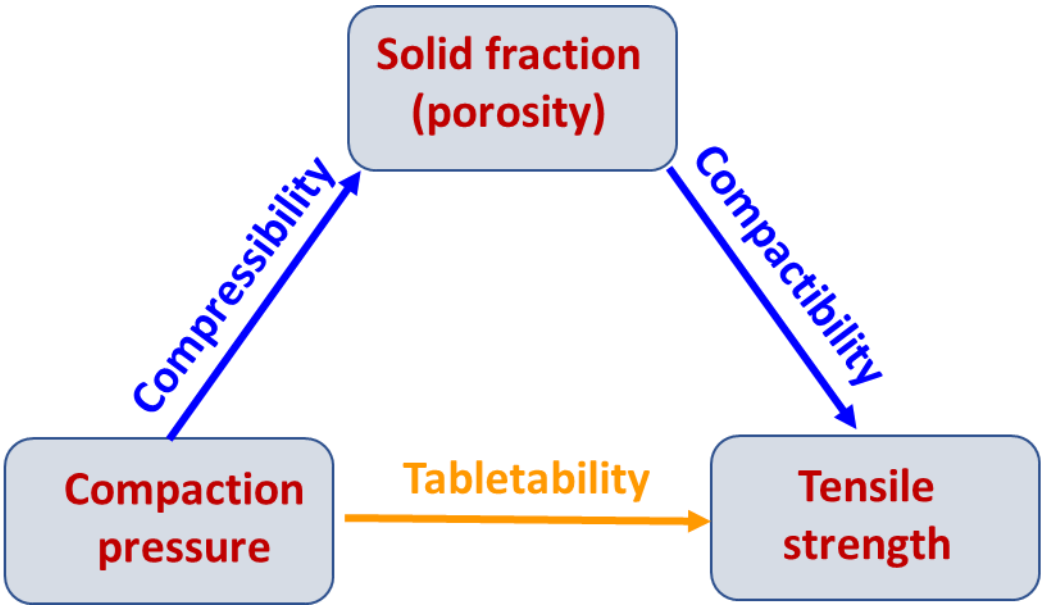

Figure 1.1 relationships among compaction pressure, tensile strength, and solid fraction

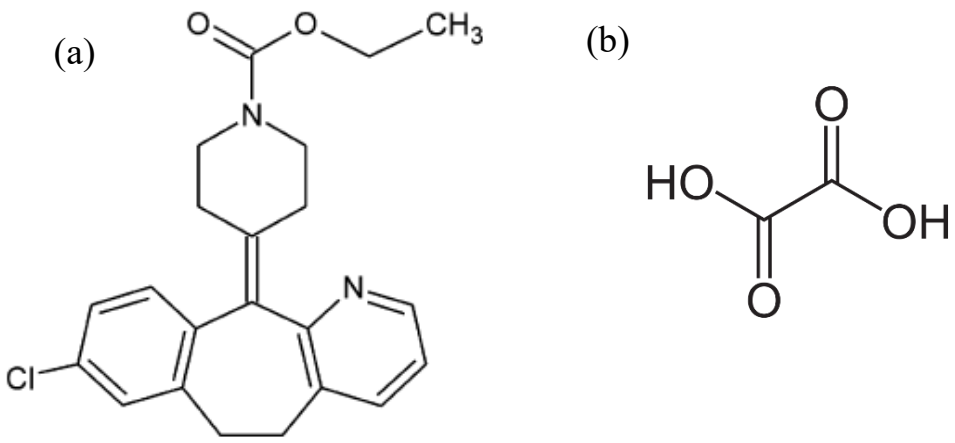

Figure 2.1. Chemical structures of (a) Loratadine (MW=382.88 g/mol) and (b) Oxalic acid (MW=90.04 g/mol)

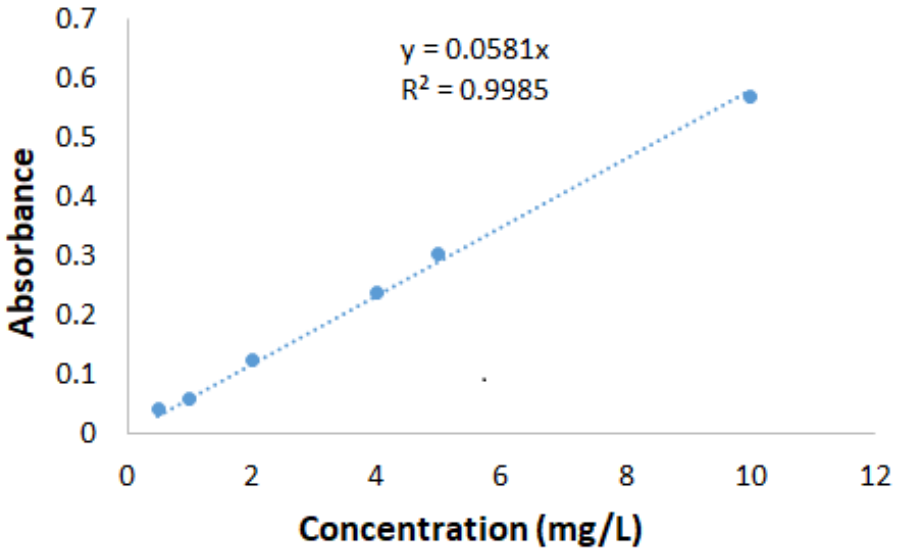

Figure 2.2. Standard curve of Lor in PH=6.8 phosphate buffer

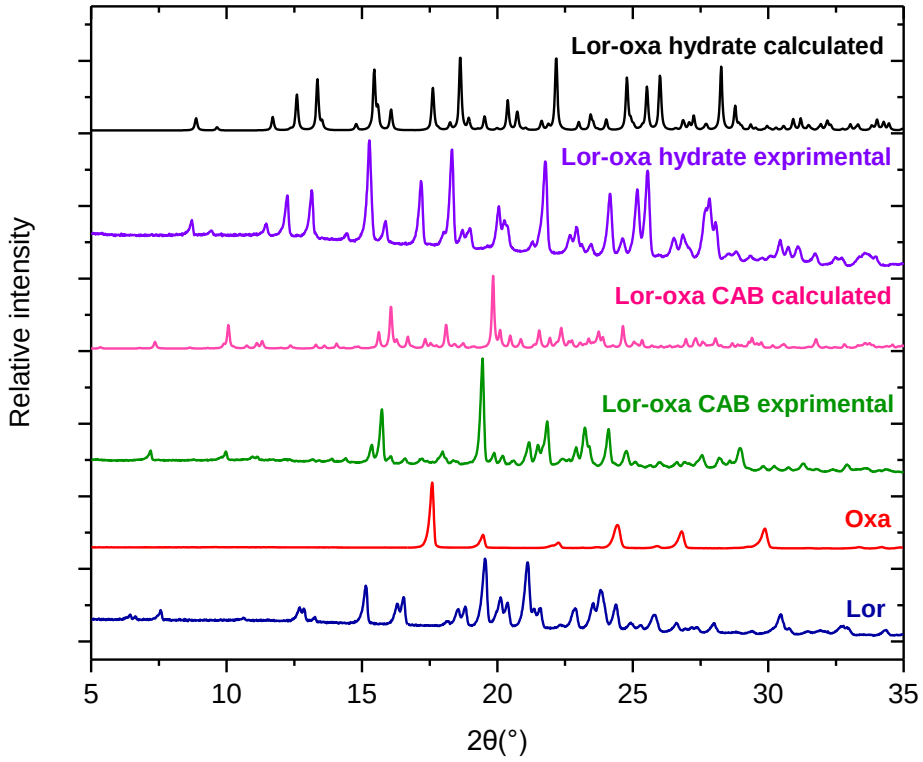

Figure 2.3. Experimental PXRD patterns of Lor, Oxa, Lor-Oxa CAB, Lor-Oxa hydrate, and calculated PXRD patterns of Lor-Oxa CAB, and Lor-Oxa hydrate

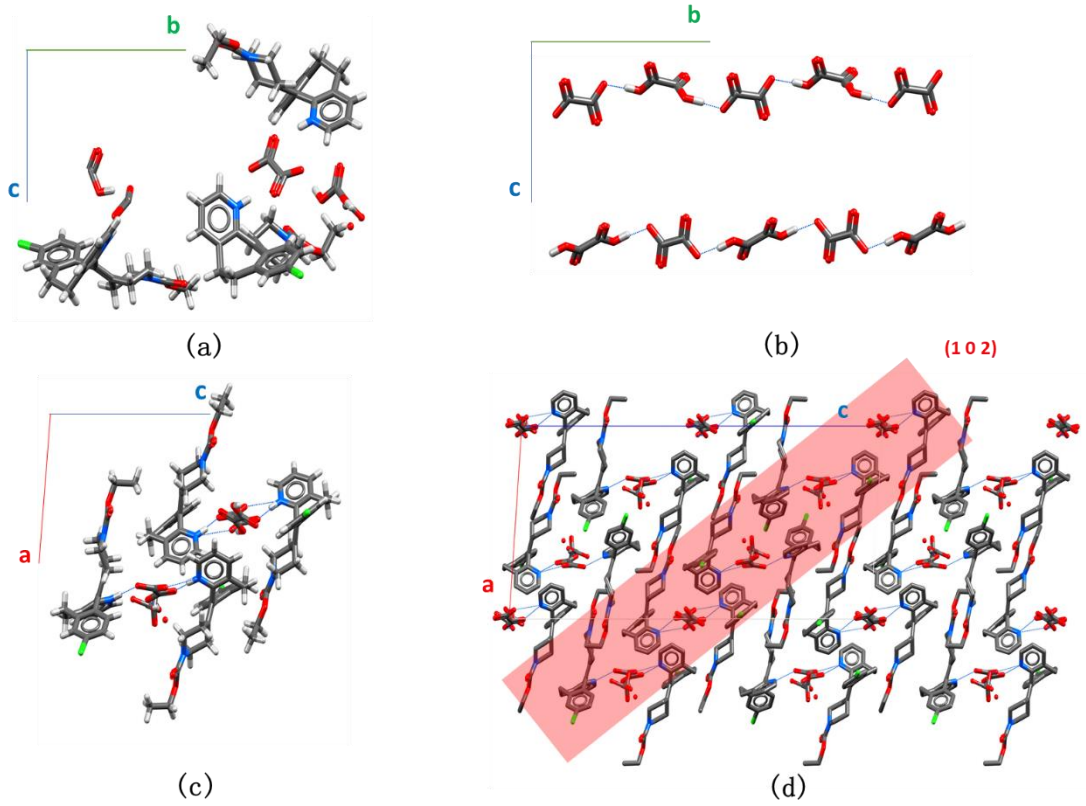

Figure 2.4 Crystal structure of Lor-Oxa CAB: (a) asymmetric unit; (b) oxalic acid chains; (c) 2D layered structure and (d) 3D packing pattern

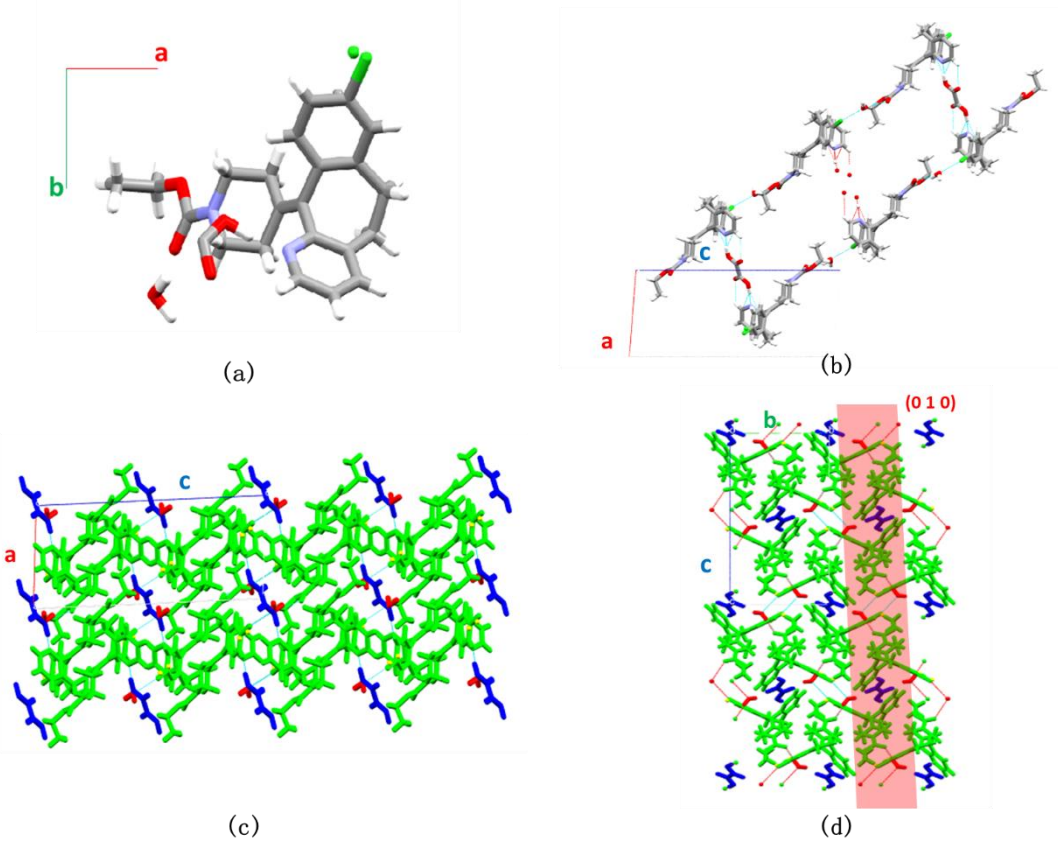

Figure 2.5. Crystal structure of Lor-Oxa hydrate: (a) asymmetric unit;(b) Lor-water chains bonded via Oxa; (c) 2D layered structure, and (d) 3D packing pattern

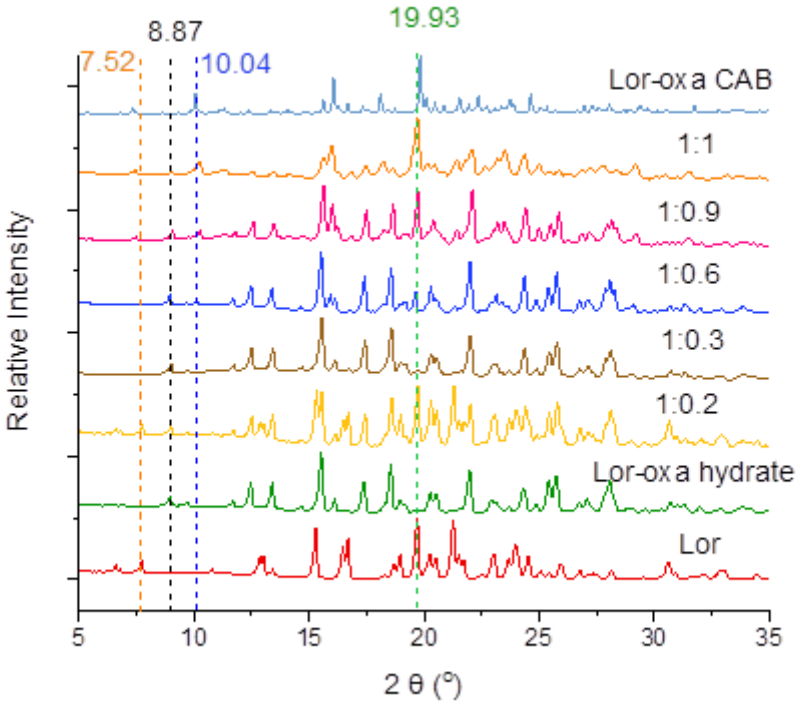

Figure 2.6. Effects of Oxa amount on phase change during slurry experiments. Lor to Oxa ratios are given.

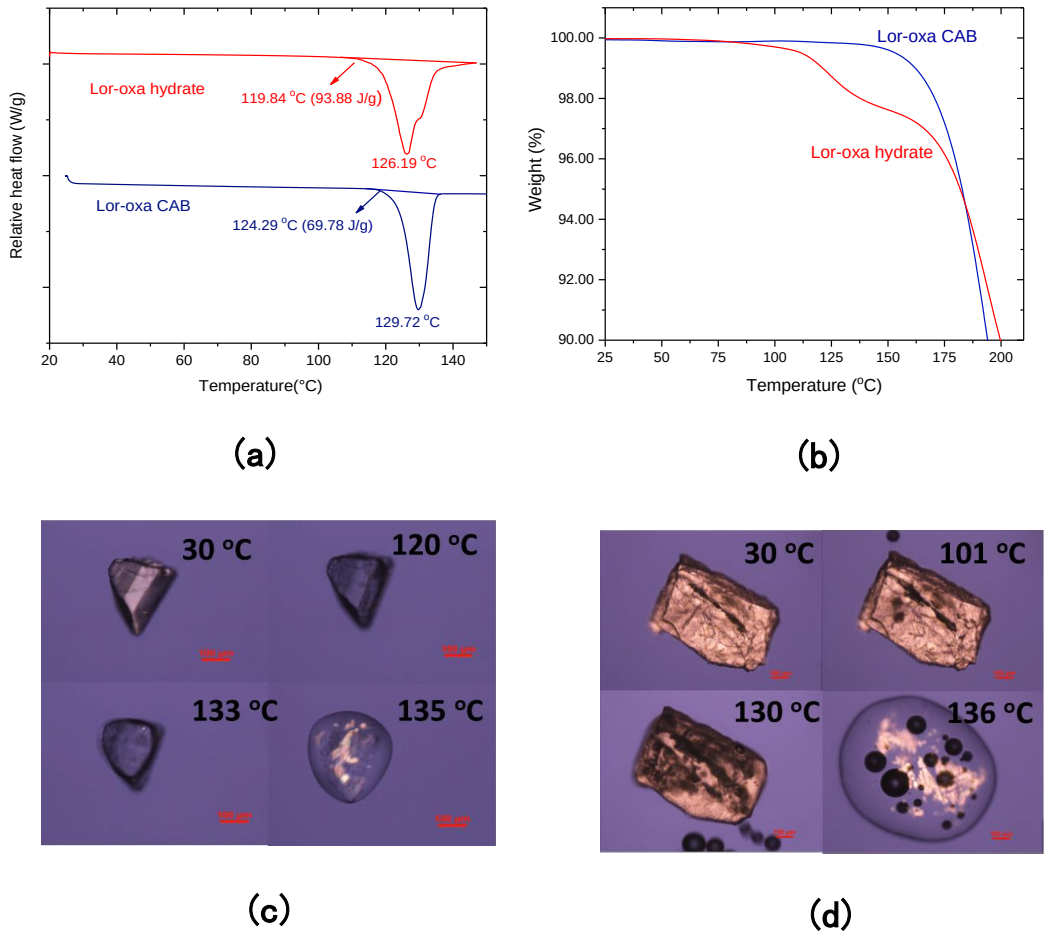

Figure 2.7 Thermal analysis of Lor-Oxa CAB and Lor-Oxa hydrate: (a) DSC, (b) TGA and HSM of (c) Lor-Oxa CAB and (d) Lor-Oxa hydrate.

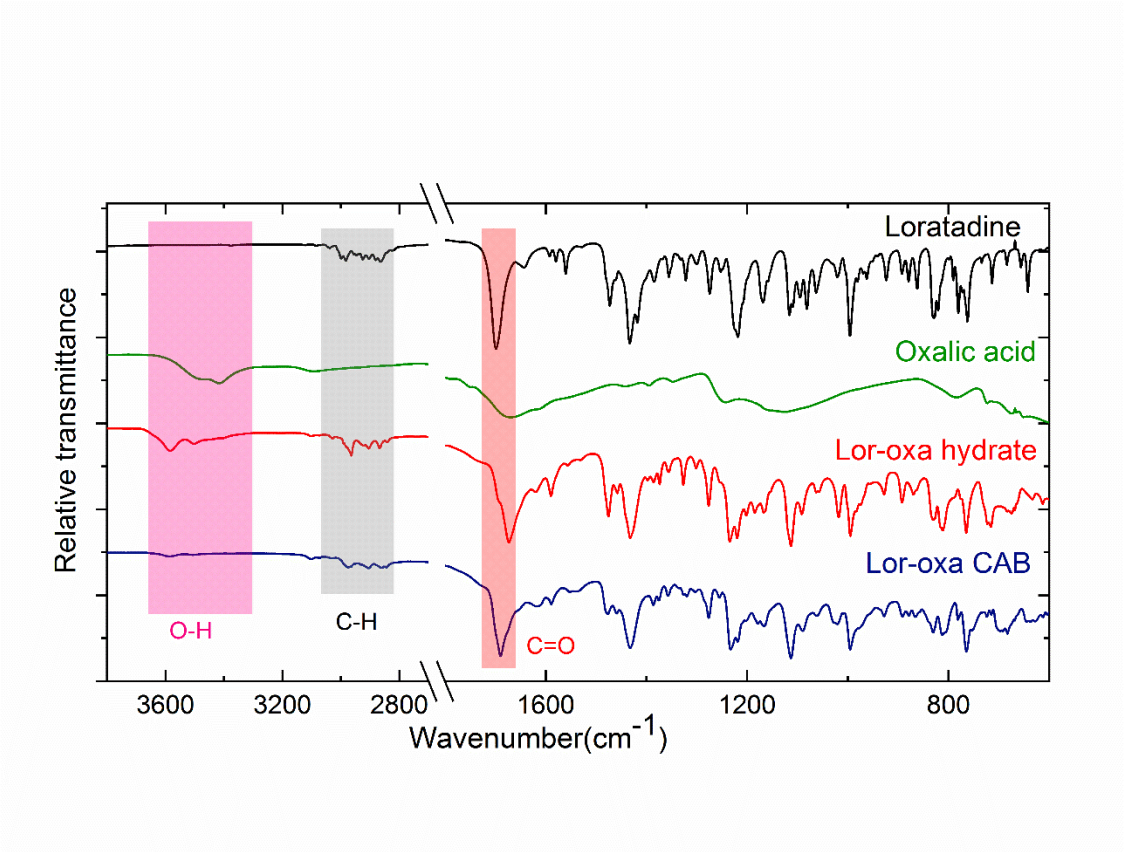

Figure 2.8. FTIR spectra of Lor, Oxa, Lor-Oxa CAB, and Lor-Oxa hydrate

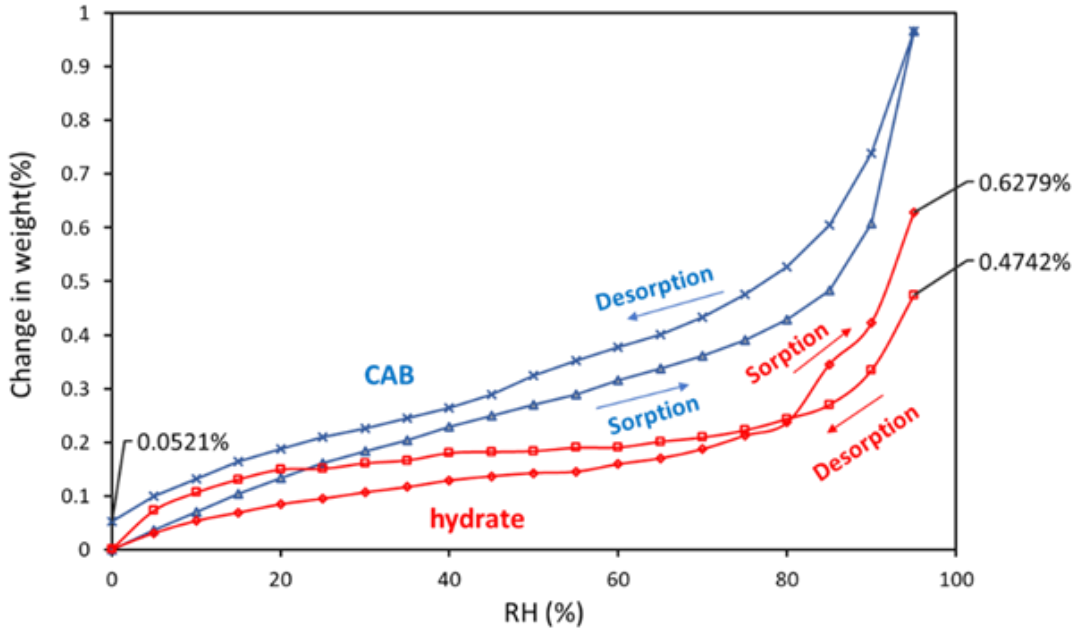

Figure 2.9. Moisture desorption and sorption isotherms of Lor-Oxa CAB (sorption followed by desorption) and Lor-Oxa hydrate (desorption followed by sorption)

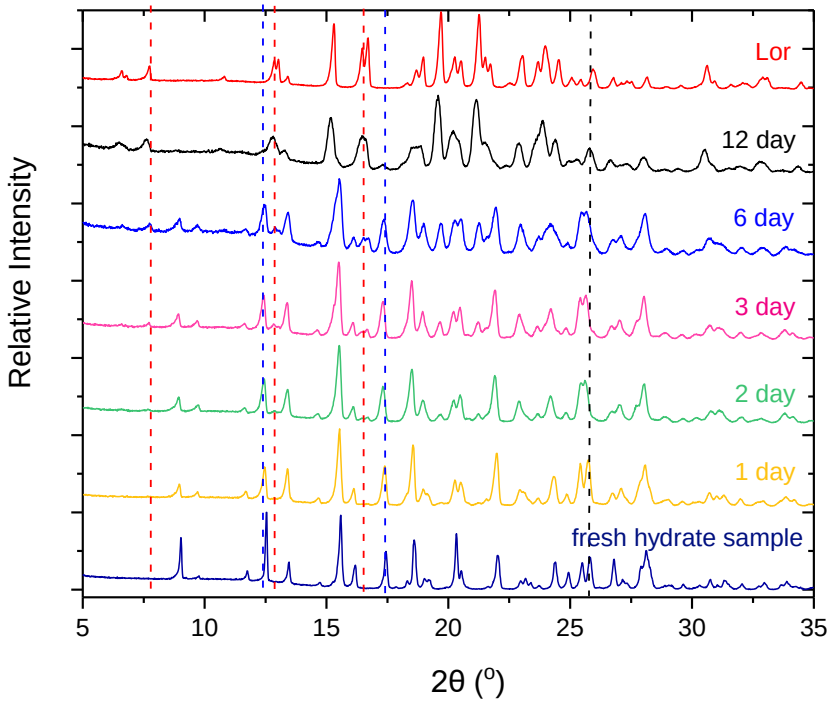

Figure 2.10. PXRD patterns of Lor-Oxa hydrate powder stored at 100°C

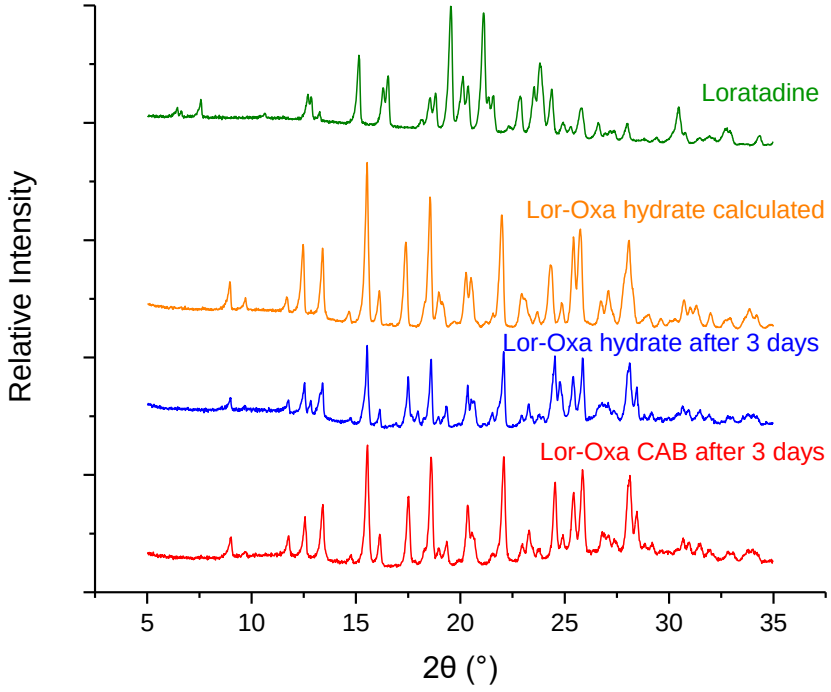

Figure 2.11. PXRD patterns of Lor-Oxa CAB and Lor-Oxa hydrate powders after solubility study in phosphate buffer.

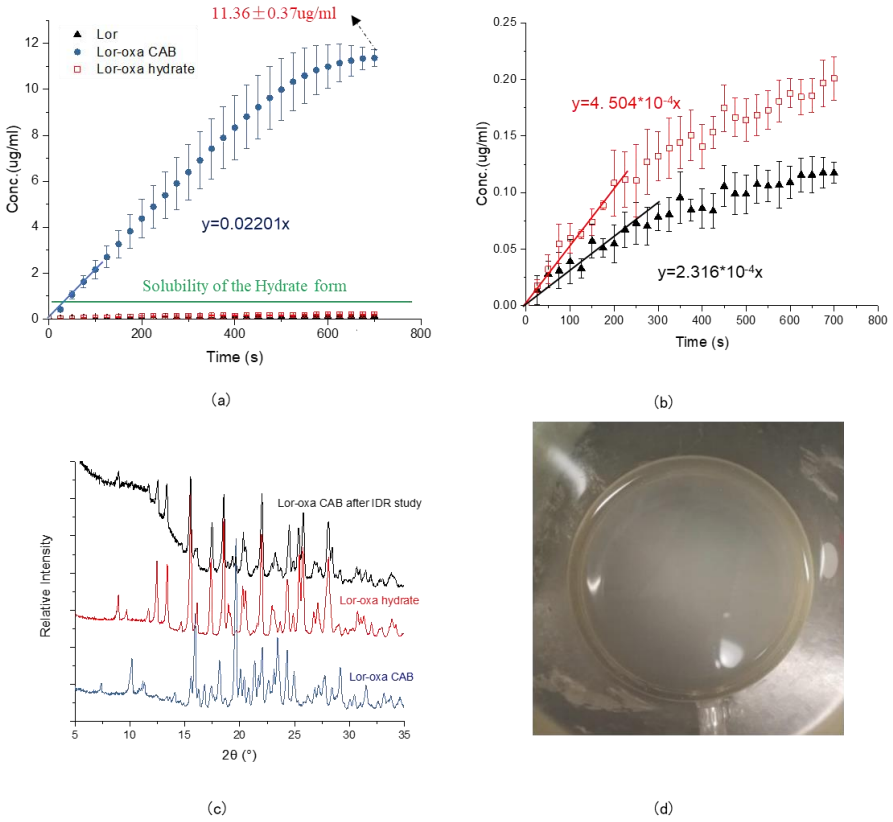

Figure 2.12. (a) IDR of Lor, Lor-Oxa CAB, and Lor-Oxa hydrate, (b) IDR of Lor and Lor-Oxa hydrate, (c) PXRD pattern of Lor-Oxa CAB pellet after IDR study in comparision to those of Lor-Oxa CAB and Lor-Oxa hydrate, and (d) turbid bulk medium after IDR experiment.

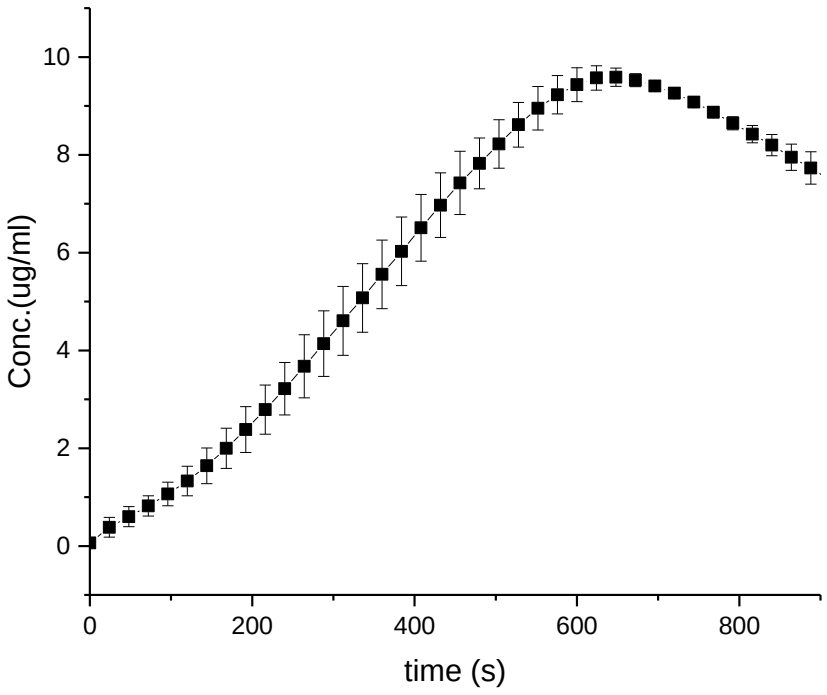

Figure 2.13. IDR profile of Lor-Oxa CAB in the first 15 min.

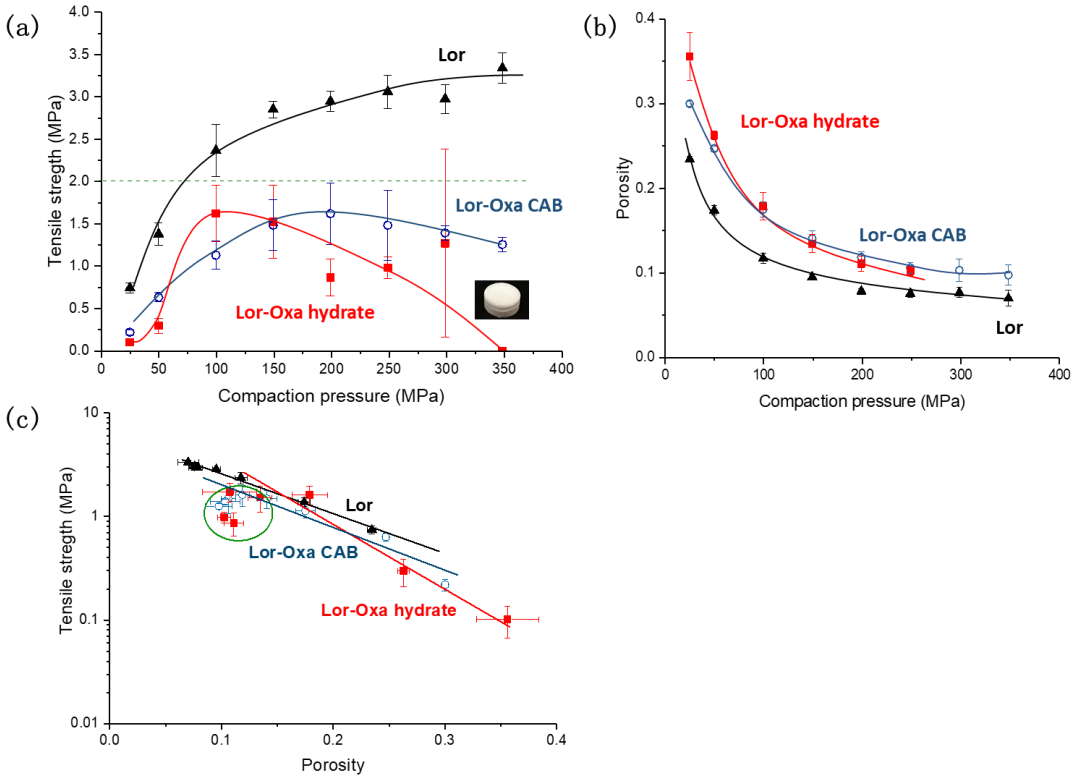

Figure 2.14. (a) Tabletability, (b) compressibility, and (c) compatibility profiles of Lor, Lor-Oxa CAB, and Lor-Oxa hydrate

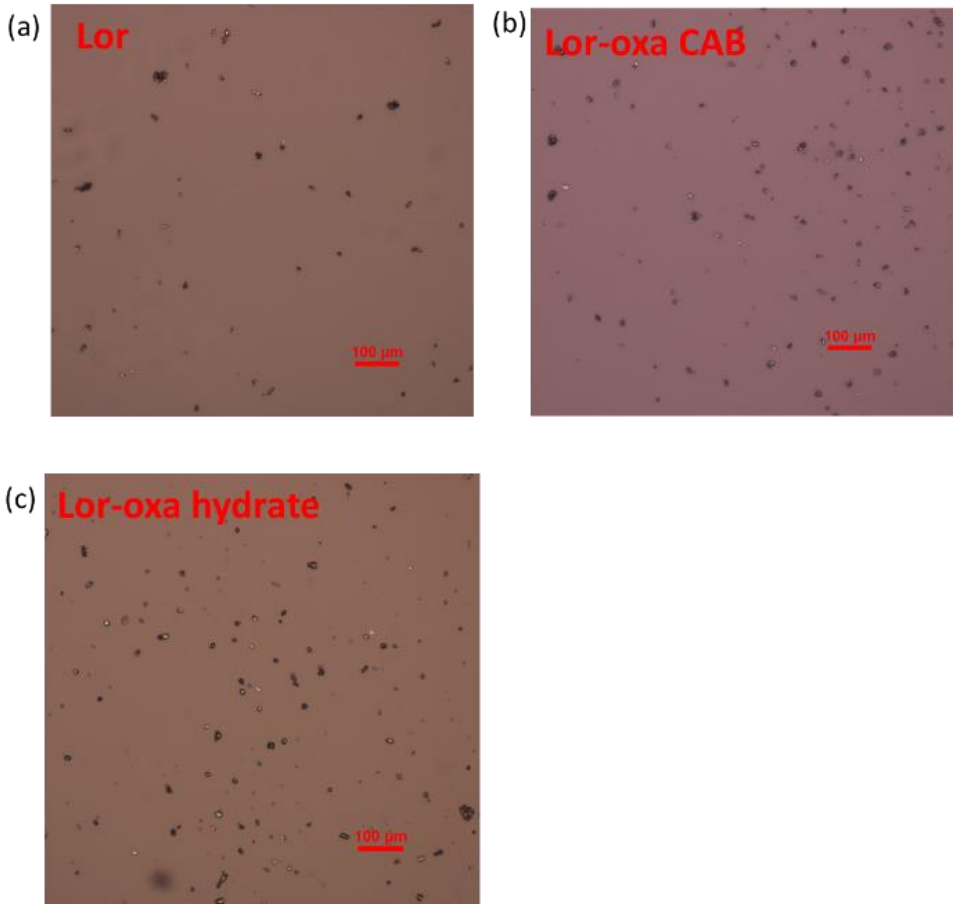

Figure 2.15. PLM images of (a) Lor, (b) Lor-Oxa CAB, and (c) Lor-Oxa hydrate for powders used for tablet compression

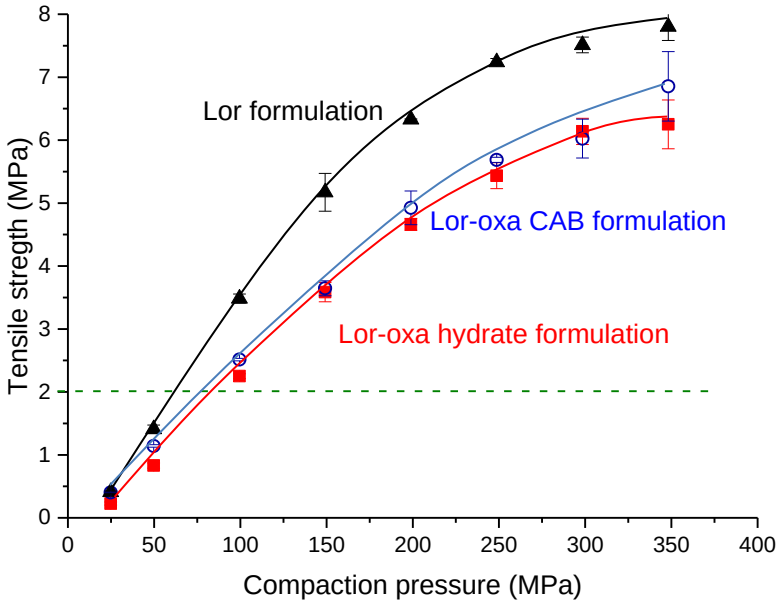

Figure 2.16. Tabletability profiles of Lor, Lor-Oxa CAB, and Lor-Oxa hydrate formulations. The formulation is comprised of 25% of one of the three Lor crystals and 75% MCC (w/w).

CHAPTER 3.

RESEARCH SUMMARY AND FUTURE WORK

3.1 Research Summary

Two new multi-component crystalline forms of Lor with oxalic acid were discovered, i.e., , a 1:1 Loratadine - oxalic acid conjugate acid-base salt (Lor-Oxa CAB) and a 2:1 Loratadine - oxalic acid monohydrate (Lor-Oxa hydrate). Crystal structures of both crystals were solved using single crystal X-ray diffraction, and the solid-state properties, tabletability, solubility, and intrinsic dissolution rate (IDR) were characterized. Both crystals show enhanced solubility and dissolution behavior over Lor, while Lor-Oxa CAB exhibited an IDR that is about 95 times higher than Lor. Both new crystal forms could be suitable for use in tablet formulation development, but Lor-Oxa CAB is preferred due to its higher solubility and better compression properties.

3.2 Future Work

Bulk precipitation phenomenon was observed on Lor-Oxa CAB during IDR study. Further exploration of the mechanism of this phenomenon may guide the development of a fast release and robust tablet formulation using Lor-Oxa CAB. It is also a good model system to gain fundamental insight into the factors that control the precipitation during dissolution. This is of value because soluble salts of the poorly soluble APIs tend to dissociate during the dissolution process in GI fluids. Precipitation can occur either on the tablet surface or in the bulk media based on different mechanisms. During bulk precipitation, the poorly soluble drug precipitates out from the bulk medium, creating a suspension. However, this phenomenon is rare because the driving force for

precipitation is usually higher at the surface of dissolving particles.

References

1. Aulton, M. E., *Pharmaceutics: The science of dosage form design*. Churchill livingstone: 2002.
2. Sun, C. C.; Hou, H.; Gao, P.; Ma, C.; Medina, C.; Alvarez, F. J., Development of a high drug load tablet formulation based on assessment of powder manufacturability: moving towards quality by design. *J Pharm Sci* **2009,** *98* (1), 239-47.
3. Sun, C. C., Materials science tetrahedron—A useful tool for pharmaceutical research and development. *Journal of pharmaceutical sciences* **2009,** *98* (5), 1671-1687.
4. Perumalla, S. R.; Paul, S.; Sun, C. C., Enabling the tablet product development of 5-fluorocytosine by conjugate acid base cocrystals. *Journal of pharmaceutical sciences* **2016,** *105* (6), 1960-1966.
5. Sun, C. C., Decoding Powder Tabletability: Roles of Particle Adhesion and Plasticity. *Journal of Adhesion Science and Technology* **2011,** *25* (4-5), 483-499.
6. Simons, F. E., Advances in H1-antihistamines. *The New England journal of medicine* **2004,** *351* (21), 2203-17.
7. Clark, M. J.; Million, R. P., Allergic rhinitis: market evolution. Nature Publishing Group: 2009.
8. Berry, D. J.; Steed, J. W., Pharmaceutical cocrystals, salts and multicomponent systems; intermolecular interactions and property based design. *Advanced Drug Delivery Reviews* **2017,** *117*, 3-24.
9. Aitipamula, S.; Banerjee, R.; Bansal, A. K.; Biradha, K.; Cheney, M. L.; Choudhury, A. R.; Desiraju, G. R.; Dikundwar, A. G.; Dubey, R.; Duggirala, N.; Ghogale, P. P.; Ghosh, S.; Goswami, P. K.; Goud, N. R.; Jetti, R. R. K. R.; Karpinski, P.; Kaushik, P.; Kumar, D.; Kumar, V.; Moulton, B.; Mukherjee, A.; Mukherjee, G.; Myerson, A. S.; Puri, V.; Ramanan, A.; Rajamannar, T.; Reddy, C. M.; Rodriguez-Hornedo, N.; Rogers, R. D.; Row, T. N. G.; Sanphui, P.; Shan, N.; Shete, G.; Singh, A.; Sun, C. C.; Swift, J. A.; Thaimattam, R.; Thakur, T. S.; Kumar Thaper, R.; Thomas, S. P.; Tothadi, S.; Vangala, V. R.; Variankaval, N.; Vishweshwar, P.; Weyna, D. R.; Zaworotko, M. J., Polymorphs, Salts, and Cocrystals: What's in a Name? *Crystal Growth & Design* **2012,** *12* (5), 2147-2152.
10. Desiraju, G. R.; Parshall, G. W., Crystal engineering: the design of organic solids. *Materials science monographs* **1989,** *54*.
11. Mittal, B., Chapter 2 - Pharmacokinetics and Preformulation. In *How to Develop Robust Solid Oral Dosage Forms from Conception to Post-Approval*, Mittal, B., Ed. Academic Press: 2017; pp 17-37.
12. Taskinen, J.; Norinder, U., 5.26 - In Silico Predictions of Solubility. In *Comprehensive Medicinal Chemistry II*, Taylor, J. B.; Triggle, D. J., Eds. Elsevier: Oxford, 2007; pp 627-648.
13. Ishikawa, M.; Hashimoto, Y., Chapter 31 - Improving the Water-Solubility of Compounds by Molecular Modification to Disrupt Crystal Packing. In *The Practice of Medicinal Chemistry (Fourth Edition)*, Wermuth, C. G.; Aldous, D.; Raboisson, P.; Rognan, D., Eds. Academic Press: San Diego, 2015; pp 747-765.
14. Grant, D. J. W.; Higuchi, T., *Solubility behavior of organic compounds*. John Wiley & Sons: 1990.
15. Smith, B. T., *Remington education: physical pharmacy*. Pharmaceutical Press: 2015.
16. Noyes, A. A.; Whitney, W. R., The rate of solution of solid substances in their own solutions. *Journal of the American Chemical Society* **1897,** *19* (12), 930-934.
17. Hamlin, W. E.; Northam, J. I.; Wagner, J. G., Relationship between in vitro dissolution rates and solubilities of numerous compounds representative of various chemical species. *Journal of Pharmaceutical Sciences* **1965,** *54* (11), 1651-1653.
18. Rasenack, N.; Müller, B. W., Dissolution rate enhancement by in situ micronization of poorly

water-soluble drugs. *Pharmaceutical research* **2002,** *19* (12), 1894-1900.

19. Prakongpan, S.; Higuchi, W.; Kwan, K.; Molokhia, A., Dissolution rate studies of cholesterol monohydrate in bile acid – lecithin solutions using the rotating - disk method. *Journal of pharmaceutical sciences* **1976,** *65* (5), 685-689.

20. Lawrence, X. Y.; Carlin, A. S.; Amidon, G. L.; Hussain, A. S., Feasibility studies of utilizing disk intrinsic dissolution rate to classify drugs. *International journal of pharmaceutics* **2004,** *270* (1-2), 221-227.

21. Nikolakakis, I.; Partheniadis, I., Self-Emulsifying Granules and Pellets: Composition and Formation Mechanisms for Instant or Controlled Release. *Pharmaceutics* **2017,** *9*, 50.

22. Williams, H. D.; Trevaskis, N. L.; Charman, S. A.; Shanker, R. M.; Charman, W. N.; Pouton, C. W.; Porter, C. J., Strategies to address low drug solubility in discovery and development. *Pharmacol Rev* **2013,** *65* (1), 315-499.

23. Ansel, H. C.; Popovich, N. G.; Allen, L. V., *Pharmaceutical dosage forms and drug delivery systems*. Williams & Wilkins Baltimore: 1995; Vol. 6.

24. Jivraj, M.; Martini, L. G.; Thomson, C. M., An overview of the different excipients useful for the direct compression of tablets. *Pharmaceutical Science & Technology Today* **2000,** *3* (2), 58-63.

25. Mittal, K. L.; Etzler, F. M., *Adhesion in pharmaceutical, biomedical, and dental fields*. John Wiley & Sons: 2017.

26. Davies, P., Oral solid dosage forms. In *Pharmaceutical preformulation and formulation*, CRC Press: 2015; pp 391-470.

27. Conine, J. W.; Pikal, M. J., Special tablets. *Pharmaceutical Dosage Forms: Tablets* **1989,** *1*, 329.

28. Yamashita, H.; Sun, C. C., Expedited Tablet Formulation Development of a Highly Soluble Carbamazepine Cocrystal Enabled by Precipitation Inhibition in Diffusion Layer. *Pharmaceutical research* **2019,** *36* (6), 90.

29. Sun, C. C.; Hou, H., Improving mechanical properties of caffeine and methyl gallate crystals by cocrystallization. *Crystal Growth and Design* **2008,** *8* (5), 1575-1579.

30. Porter, S.; Sackett, G.; Liu, L., Development, optimization, and scale-up of process parameters: pan coating. In *Developing solid oral dosage forms*, Elsevier: 2017; pp 953-996.

31. Sun, C.; Grant, D. J., Influence of crystal structure on the tableting properties of sulfamerazine polymorphs. *Pharmaceutical research* **2001,** *18* (3), 274-280.

32. Tye, C. K.; Sun, C.; Amidon, G. E., Evaluation of the effects of tableting speed on the relationships between compaction pressure, tablet tensile strength, and tablet solid fraction. *Journal of Pharmaceutical Sciences* **2005,** *94* (3), 465-472.

33. Pepinsky, R. In *Crystal engineering-new concept in crystallography*, Physical Review, AMERICAN PHYSICAL SOC ONE PHYSICS ELLIPSE, COLLEGE PK, MD 20740-3844 USA: 1955; pp 971-971.

34. Schmidt, G., Photodimerization in the solid state. *Pure and Applied Chemistry* **1971,** *27* (4), 647-678.

35. Reddy, D. S.; Ovchinnikov, Y. E.; Shishkin, O. V.; Struchkov, Y. T.; Desiraju, G. R., Supramolecular Synthons in Crystal Engineering. 3. Solid State Architecture and Synthon Robustness in Some 2,3-Dicyano-5,6-dichloro-1,4-dialkoxybenzenes1. *Journal of the American Chemical Society* **1996,** *118* (17), 4085-4089.

36. Thakuria, R.; Nangia, A., Highly soluble olanzapinium maleate crystalline salts. *CrystEngComm* **2011,** *13* (6), 1759-1764.

37. Blagden, N.; de Matas, M.; Gavan, P. T.; York, P., Crystal engineering of active pharmaceutical

ingredients to improve solubility and dissolution rates. *Advanced drug delivery reviews* **2007,** *59* (7), 617-630.

38. Perumalla, S. R.; Sun, C. C., Improved solid-state stability of salts by cocrystallization between conjugate acid–base pairs. *CrystEngComm* **2013,** *15* (29), 5756-5759.

39. Deng, J.-H.; Lu, T.-B.; Sun, C. C.; Chen, J.-M., Dapagliflozin-citric acid cocrystal showing better solid state properties than dapagliflozin. *European Journal of Pharmaceutical Sciences* **2017,** *104*, 255-261.

40. Wang, C.; Tong, Q.; Hou, X.; Hu, S.; Fang, J.; Sun, C. C., Enhancing bioavailability of dihydromyricetin through inhibiting precipitation of soluble cocrystals by a crystallization inhibitor. *Crystal Growth & Design* **2016,** *16* (9), 5030-5039.

41. Yamashita, H.; Sun, C. C., Improving dissolution rate of carbamazepine-glutaric acid cocrystal through solubilization by excess coformer. *Pharmaceutical research* **2018,** *35* (1), 4.

42. Yan, Y.; Chen, J.-M.; Lu, T.-B., Simultaneously enhancing the solubility and permeability of acyclovir by crystal engineering approach. *CrystEngComm* **2013,** *15* (33), 6457-6460.

43. Wang, C.; Paul, S.; Sun, D. J.; Nilsson Lill, S. O.; Sun, C. C., Mitigating punch sticking propensity of celecoxib by cocrystallization–an integrated computational and experimental approach. *Crystal Growth & Design* **2020**.

44. Bučar, D.-K.; Filip, S.; Arhangelskis, M.; Lloyd, G. O.; Jones, W., Advantages of mechanochemical cocrystallisation in the solid-state chemistry of pigments: colour-tuned fluorescein cocrystals. *CrystEngComm* **2013,** *15* (32), 6289-6291.

45. Etter, M. C., Encoding and decoding hydrogen-bond patterns of organic compounds. *Accounts of Chemical Research* **1990,** *23* (4), 120-126.

46. Vieth, M.; Siegel, M. G.; Higgs, R. E.; Watson, I. A.; Robertson, D. H.; Savin, K. A.; Durst, G. L.; Hipskind, P. A., Characteristic Physical Properties and Structural Fragments of Marketed Oral Drugs. *Journal of Medicinal Chemistry* **2004,** *47* (1), 224-232.

47. Sun, C. C., Cocrystallization for successful drug delivery. *Expert opinion on drug delivery* **2013,** *10* (2), 201-213.

48. Chen, H.; Guo, Y.; Wang, C.; Dun, J.; Sun, C. C., Spherical Cocrystallization—An Enabling Technology for the Development of High Dose Direct Compression Tablets of Poorly Soluble Drugs. *Crystal Growth & Design* **2019,** *19* (4), 2503-2510.

49. Popović, G.; Čakar, M.; Agbaba, D., Acid–base equilibria and solubility of loratadine and desloratadine in water and micellar media. *Journal of Pharmaceutical and Biomedical Analysis* **2009,** *49* (1), 42-47.

50. Khan, M. Z. I.; Rau; x; l, D.; Zano; x; ki, R.; x17E; ica; Zidar, S.; x17E; ana; Mikul; x10D; x; Horvat, J.; Krizmani; x; Lara; x; kinja, M.; Mildner, B.; Kne; x17E; evi; x; Zdravka, Classification of Loratadine Based on the Biopharmaceutics Drug Classification Concept and Possible in Vitro–in Vivo Correlation. *Biological and Pharmaceutical Bulletin* **2004,** *27* (10), 1630-1635.

51. Sora, D. I.; Udrescu, S.; David, V.; Medvedovici, A., Validated ion pair liquid chromatography/fluorescence detection method for assessing the variability of the loratadine metabolism occurring in bioequivalence studies. *Biomed Chromatogr* **2007,** *21* (10), 1023-9.

52. Zhang, S.; Sun, M.; Zhao, Y.; Song, X.; He, Z.; Wang, J.; Sun, J., Molecular mechanism of polymer-assisting supersaturation of poorly water-soluble loratadine based on experimental observations and molecular dynamic simulations. *Drug Deliv Transl Res* **2017,** *7* (5), 738-749.

53. Kuminek, G.; Cavanagh, K. L.; da Piedade, M. F. M.; Rodríguez-Hornedo, N., Posaconazole Cocrystal with Superior Solubility and Dissolution Behavior. *Crystal Growth & Design* **2019,** *19* (11),

6592-6602.

54. Nacsa, A.; Ambrus, R.; Berkesi, O.; Szabo-Revesz, P.; Aigner, Z., Water-soluble loratadine inclusion complex: analytical control of the preparation by microwave irradiation. *J Pharm Biomed Anal* **2008,** *48* (3), 1020-3.

55. Lin, S.-Y.; Hsu, C.-H.; Sheu, M.-T., Curve-fitting FTIR studies of loratadine/hydroxypropyl-β-cyclodextrin inclusion complex induced by co-grinding process. *Journal of Pharmaceutical and Biomedical Analysis* **2010,** *53* (3), 799-803.

56. Frizon, F.; Eloy, J. d. O.; Donaduzzi, C. M.; Mitsui, M. L.; Marchetti, J. M., Dissolution rate enhancement of loratadine in polyvinylpyrrolidone K-30 solid dispersions by solvent methods. *Powder Technology* **2013,** *235*, 532-539.

57. Bandari, S.; Jadav, S.; Eedara, B. B.; Dhurke, R.; Jukanti, R., Enhancement of Solubility and Dissolution Rate of Loratadine with Gelucire 50/13. *Journal of Pharmaceutical Innovation* **2014,** *9* (2), 141-149.

58. Milak, S.; Medlicott, N.; Tucker, I. G., Solid lipid microparticles containing loratadine prepared using a Micromixer. *Journal of Microencapsulation* **2006,** *23* (8), 823-831.

59. Üner, M.; Karaman, E. F.; Aydoğmuş, Z., Solid Lipid Nanoparticles and Nanostructured Lipid Carriers of Loratadine for Topical Application: Physicochemical Stability and Drug Penetration through Rat Skin. *Tropical Journal of Pharmaceutical Research* **2014,** *13* (5).

60. Madhav, K. V.; Kishan, V., Self microemulsifying particles of loratadine for improved oral bioavailability: preparation, characterization and in vivo evaluation. *Journal of Pharmaceutical Investigation* **2018,** *48* (4), 497-508.

61. Wang, J.; Chang, R.; Zhao, Y.; Zhang, J.; Zhang, T.; Fu, Q.; Chang, C.; Zeng, A., Coamorphous Loratadine-Citric Acid System with Enhanced Physical Stability and Bioavailability. *AAPS PharmSciTech* **2017,** *18* (7), 2541-2550.

62. Alatas, F.; Aprilliana, M.; Gozali, D., The Preparation And Solubility Of Loratadine-Fumaric Acid Binary Mixture. *Asian Journal of Pharmaceutical and Clinical Research* **2016,** *10* (1).

63. Wang, C.; Perumalla, S. R.; Lu, R.; Fang, J.; Sun, C. C., Sweet Berberine. *Crystal Growth & Design* **2016,** *16* (2), 933-939.

64. Wen, H.; Wang, C.; Sun, C. C., Fast Determination of Phase Stability of Hydrates Using Intrinsic Dissolution Rate Measurements. *Crystal Growth & Design* **2019,** *19* (10), 5471-5476.

65. Fell, J. T.; Newton, J. M., Determination of Tablet Strength by the Diametral-Compression Test. *Journal of Pharmaceutical Sciences* **1970,** *59* (5), 688-691.

66. Leane, M.; Pitt, K.; Reynolds, G., A proposal for a drug product Manufacturing Classification System (MCS) for oral solid dosage forms. *Pharmaceutical development and technology* **2015,** *20* (1), 12-21.

67. Wang, C.; Chopade, S. A.; Guo, Y.; Early, J. T.; Tang, B.; Wang, E.; Hillmyer, M. A.; Lodge, T. P.; Sun, C. C., Preparation, characterization, and formulation development of drug–drug protic ionic liquids of diphenhydramine with ibuprofen and naproxen. *Molecular pharmaceutics* **2018,** *15* (9), 4190-4201.

68. Good, D. J.; Rodríguez-Hornedo, N. r., Solubility Advantage of Pharmaceutical Cocrystals. *Crystal Growth & Design* **2009,** *9* (5), 2252-2264.

69. Chen, H.; Aburub, A.; Sun, C. C., Direct Compression Tablet Containing 99% Active Ingredient—A Tale of Spherical Crystallization. *Journal of Pharmaceutical Sciences* **2019,** *108* (4), 1396-1400.

70. Paul, S.; Sun, C. C., Gaining insight into tablet capping tendency from compaction simulation. *International Journal of Pharmaceutics* **2017,** *524* (1), 111-120.

71. Osei-Yeboah, F.; Chang, S.-Y.; Sun, C. C., A critical examination of the phenomenon of bonding area-bonding strength interplay in powder tableting. *Pharmaceutical research* **2016,** *33* (5), 1126-1132.